Direct Numerical Simulations of imploding & expanding flames. Effects of steam dilution, turbulence and Lewis number.

Eric Albin[a,b], Christian Oliver Paschereit[b], Yves D'Angelo[c]
eric.albin@univ-lyon1.fr
[a] Chair of Fluid Dynamics, Technische Universität Berlin
Müller-Breslau-Str. 8 10623 Berlin, Germany
[b] Université de Lyon, CNRS
Université Lyon 1, F-69622, France
INSA-Lyon, CETHIL, UMR5008, F-69621, Villeurbanne, France
[c] INSA de Rouen, CNRS
INSA/CORIA, UMR6614, 76801 St Etienne du Rouvray, Rouen, France

Abstract
A set of 20 three-dimensional Direct Numerical Simulations is computed and analysed. Imploding and expanding spherical flames of steam-methane-hydrogen-air mixtures are simulated using a single step chemistry whose coefficients are set using complex chemistry. Both turbulent and laminar cases are performed. The total flame surface and internal volume of gases are extracted from these simulations. The mean consumption speed and flame speed are determined for laminar and turbulent flames. A particular attention is given to describe the effect of high steam content, turbulence and fuels on flame speeds and flame topologies.

1 Introduction
The injection of steam into the combustion chamber have some interests for instance in humid gas turbines [1, 2]. The recovery of waste heat from exhaust gases to generate the steam that is injected into the combustion chamber significantly improve the efficiency of the cycle [2]. In [3], up to $30\%_{mass}$ of steam into the air could be achieved for natural gas/air flames and up to 50% for hydrogen-air flames. Because the steam has a specific heat about twice higher than air [4], steam considerably decreases the flame temperature, reactions and the flame speed [5], which makes humid gas turbines more flexible to burn highly reactive fuels like hydrogen enriched fuels. In this study, Direct Numerical Simulations (DNS) of inwardly and outwardly propagating spherical flames are solved and analysed to investigate the effect of steam, turbulence and fuel type (CH_4 or H_2).

Expanding flames are encountered in numerous experiments and engines [6, 7] since the ignition of an inflammable mixture with a spark leads to the propagation of an expanding kernel; it is also well suited to be computed in Direct Numerical Simulations (DNS) [8, 9]. On the opposite, measurements on inwardly propagating spherical flames lack in the literature due to the difficulty in performing an implosive combustion [10]. Since spherical ignitions can be enforced in numerical works, imploding flames are also well suited for simulations [11, 12]. In this study, all simulations are computed at dry conditions or with 20% in mass of steam into the air to determine the effect of high steam dilution on flame speeds. Every composition is ignited both in inert flows and in turbulent flows to compare

laminar and turbulent flame propagations. Trends are compared to laminar experimental results of Lecordier [6] and Baillot *et* al. [10].

In the literature, spherical flames are in general studied to extract local burning velocity, curvature and stretch from 2D images [6, 10, 13, 7] because of measurement techniques (laser slice, integral methods like shadowgraph or Schlieren). In numerics, one dimensional or two dimensional simulations may be computed [11, 14] but will miss some multi-dimensional effects like thermodiffusive instability or 3D turbulence mechanisms. Here, the total 3D flame area and its internal volume of burnt or fresh gases are measured in time. Mean flame speed, burning velocity and flame curvature are deduced from these observations. The link between burning velocity and curvature for negative Lewis numbers (hydrogen mixtures) and unity or positive numbers (methane or propane) will be compared at wet and dry conditions.

An overview of the different simulations and corresponding settings are presented in the second section. The post-processing strategy of the large 3D data is described in a third section. Basic definitions of the consumption speed, flame speed and Markstein's length are also introduced in this part. The fourth section analyses laminar flames in expansion and implosion; turbulent flames are studied in section 5. A summary of the main observations and other perspectives are broached in the conclusion.

2 Description of simulated cases

DNS are computed using a compressible solver of Navier-Stokes equations already described in [15]. This solver makes use of a staggered arrangement to solve expanding and imploding flame kernels with a sixth order accuracy and a three-dimensional characteristic treatment of boundary conditions. Note that this treatment of acoustic waves minimizes the effect of boundary conditions in the current expanding or imploding flame configurations [16, 17]. A single step-chemistry is used to keep the cpu-cost reasonable and focus on flame dynamics with reasonable physical sizes. Fig. 1 shows a mosaic of 20 pictures representing the different imploding and expanding flames solved.

In all the computations, premixed unburnt gases are preheated to $T_u = 480K$ with a pressure $P_u = 1atm$. Such preheating temperatures are common in gas turbines or when performing experiments with steam [5, 18]. Four different mixtures are studied in these simulations: dry and wet stoichiometric methane-air ($\phi_{CH_4} = 1$, $\Omega = 0$ and $\Omega = 20\%$), dry and wet lean hydrogen-air ($\phi_{H_2} = 1$, $\Omega = 0$ and $\Omega = 20\%$), with the steam-to-air ratio Ω (also called specific humidity) representing the mass proportion of steam relative to dry air [18]. One dimensional laminar unstretched flames are first solved with a DNS

Table 1. Main settings of the mixtures used in DNS computations ($\gamma = 1.3$, $P_u = 1atm$). For all cases, $Sc_{O_2} \simeq Sc_{N_2} = 0.7$ and $Sc_{H_2O} = 0.58$.

Fuel	ϕ_F	Ω	K T_u	J/Kg/K r	10^{-5}Pa.s μ_u	α_μ	Sc_F	Pr	Le_F	m/s S_L^0	K T_b	mm δ_L^0
CH_4	1.0	0	480	318	2.54	0.666	0.7	0.692	1.00	1.05	2260	0.202
CH_4	1.0	0.2	480	352	2.35	0.73	0.7	0.701	1.00	0.41	1870	0.534
H_2	0.4	0	480	292	2.58	0.666	0.21	0.653	0.32	1.12	1580	0.163
H_2	0.4	0.2	480	322	2.38	0.73	0.21	0.674	0.31	0.36	1320	0.456

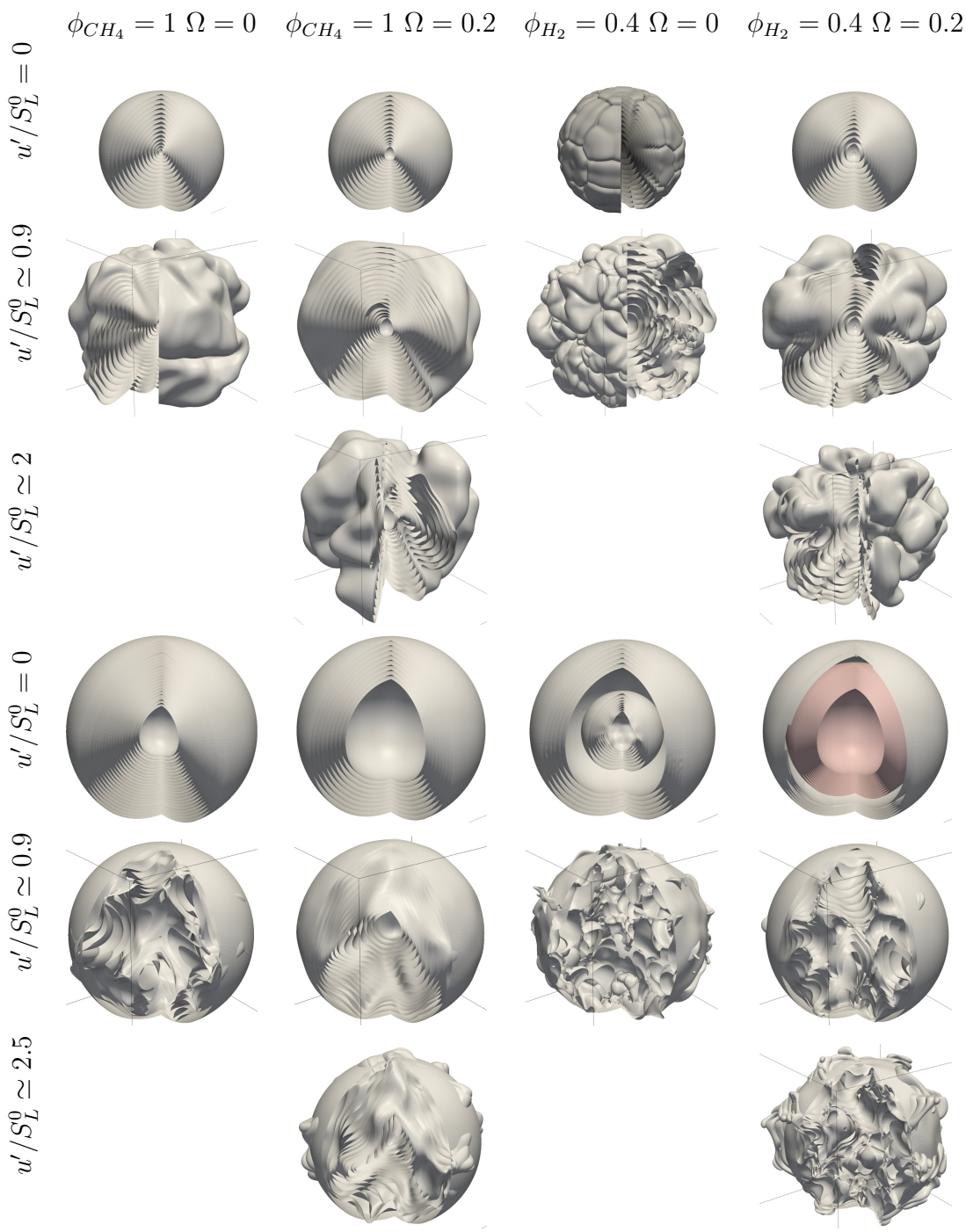

Figure 1. Mosaic illustrating the different three dimensional DNS. It represents the time-evolution of iso-temperatures of $960K$.Imploding flames are wrinkled in the center and expanding flames at large radii.

code using complex chemistry [19, 20, 21] to set transport coefficients and thermophysical properties of the single step chemistry. Table 1 shows the settings of the four mixtures and the measured flame speed, temperature of burnt gases and flame thickness.

Note that steam does not modify significantly the dynamic viscosity (here defined by

a Sutherland's law $\mu = \mu_u(T/T_u)^{\alpha_\mu}$), thermal diffusivity (see Prandtl number Pr) and mass diffusivity of species (see Schmidt numbers Sc_k). Nevertheless, high steam content decreases the molar mass and therefore the temperature of burnt gases since it increases heat capacities of the gas mixture. Detailed mechanisms show that steam also modifies reaction paths and significantly decreases the planar unstretched adiabatic flame denoted S_L^0 and increases the flame thickness ($\delta_L^0 = (T_b - T_u)/\max||\vec{\nabla}T||$).

For each of these mixtures, a laminar expanding flame and a laminar imploding flame are computed in a $(1.5cm)^3$ cubic box. This represents a total of eight simulations of 3D laminar flames. Note that expanding flame kernels are initialized using a Gaussian whereas imploding flames are defined from a hyperbolic tangent profile.

Six turbulent expanding flames and six turbulent imploding flames are also solved (see Fig. 1). The turbulence is generated from a Passot-Pouquet spectrum and then decreased in time to obtain an acceptable approximation of a decaying homogeneous isotropic turbulent field (see methodology described in [9]). The table 2 lists these different simulations and their main parameters. All these computations were carried out on an IBM Blue Gene/P system (with processors PowerPC 450) and are analysed in sections 4 and 5. They represent about 2.5 millions of cpu hours and about $10Tb$ of data to record all conserved variables in time.

Table 2. Main settings of the DNS computations.

Fuel	ϕ_F	Ω	Ignition type	$u'_{ignition}/S_L^0$	domain size	resolution	N_{proc}	cpu hours
CH_4	1.0	0	Expansion	0	$(1.5cm)^3$	336^3	512	75500
CH_4	1.0	0.2	Expansion	0	$(1.5cm)^3$	224^3	512	51100
H_2	0.4	0	Expansion	0	$(1.5cm)^3$	464^3	512	73800
H_2	0.4	0.2	Expansion	0	$(1.5cm)^3$	256^3	512	28600
CH_4	1.0	0	Implosion	0	$(1.5cm)^3$	336^3	512	49200
CH_4	1.0	0.2	Implosion	0	$(1.5cm)^3$	224^3	512	32800
H_2	0.4	0	Implosion	0	$(1.5cm)^3$	464^3	512	49200
H_2	0.4	0.2	Implosion	0	$(1.5cm)^3$	256^3	512	32800
CH_4	1.0	0	Expansion	0.854	$(1.8cm)^3$	416^3	4096	338200
CH_4	1.0	0.2	Expansion	2.09	$(1.8cm)^3$	272^3	512	100200
CH_4	1.0	0.2	Expansion	0.863	$(1.8cm)^3$	272^3	512	120600
H_2	0.4	0	Expansion	0.909	$(1.8cm)^3$	544^3	4096	294300
H_2	0.4	0.2	Expansion	1.858	$(1.7cm)^3$	288^3	512	77400
H_2	0.4	0.2	Expansion	0.889	$(1.7cm)^3$	288^3	512	82800
CH_4	1.0	0	Implosion	0.944	$(1.5cm)^3$	336^3	2048	287300
CH_4	1.0	0.2	Implosion	2.26	$(1.5cm)^3$	224^3	512	101700
CH_4	1.0	0.2	Implosion	0.841	$(1.5cm)^3$	224^3	512	98400
H_2	0.4	0	Implosion	0.871	$(1.5cm)^3$	464^3	4096	380700
H_2	0.4	0.2	Implosion	2.70	$(1.5cm)^3$	256^3	512	70040
H_2	0.4	0.2	Implosion	0.897	$(1.5cm)^3$	256^3	512	81000

Turbulent simulations are all located in flamelet regimes. Nevertheless, the thickness of the flame $\delta = D_{th}/S_L^0$ increases with steam while the dynamic viscosity μ_u of unburnt gases is few affected. Steam then tends to bring the combustion regime closer to the distributed reaction regime for a non affected turbulent field. Simulations with steam are also performed with a constant u'/S_L^0 ratio for further analysis.

3 Post-treatment method and basic definitions

These solutions represent large three dimensional data arrays saved at numerous times (Δt_{save} between 20 and $80\mu s$). In the present combustion regime, the flame front may be considered as a thin interface that propagates towards unburnt gases with a consumption speed S_C. For all recorded time-steps, the flame front is identified as an iso-contour of temperature ($960K$). The total area A of the flame front and the volume of gas V contained within this contour are systematically computed[1]. The internal volume corresponds to burnt gases ($V = V_b$) in expanding flames and to unburnt gases ($V = V_u$) for implosions. A marching cube algorithm is used for the contouring of unstructured surfaces. The radius R_A and R_V, based on the flame area and internal volume, are deduced from their definitions $A = 4\pi R_A^2$ and $V = 4\pi R_V^3/3$.

In the case of expanding flames, the mass variation $\delta m_b = \rho_b \delta V_b$ of burnt gases is equal to the consumption of a mass $\delta m_u = \rho_u \delta V_u = -\rho_u \delta A \cdot S_C dt$. In imploding flames, the volume variation δV_u of unburnt gases is simply linked to the consumption speed by $dV_u = -\delta A \cdot S_C dt$. With the assumption that the consumption speed does not vary in a nonlinear way along the flame front surface, mean consumption speeds are then computed from the whole volume and flame area, respectively for explosions and implosions :

$$S_C^{EXP} = \frac{T_u}{T_b}\frac{1}{A}\frac{dV_b}{dt} \tag{1a}$$

$$S_C^{IMP} = -\frac{1}{A}\frac{dV_u}{dt} \tag{1b}$$

A mean flame speed is also defined from the time evolution of the volume based radius:

$$S_f = \frac{dR_V}{dt} = \begin{cases} \frac{T_b}{T_u}\left(\frac{R_A}{R_V}\right)^2 \cdot S_C^{EXP} \\ -\left(\frac{R_A}{R_V}\right)^2 \cdot S_C^{IMP} \end{cases} \tag{2}$$

Note that consumption speeds are always positive while the mean flame speed is negative for implosion cases in which R_V decreases. In the literature, the consumption speed is often linearly linked to the flame curvature $\mathcal{C}$ and may deviate from the consumption speed S_L^0 of a planar unstretched adiabatic flame [22, 9]:

$$S_C = S_L^0(1 - \mathcal{L}_\mathcal{C} \cdot \mathcal{C}) \tag{3}$$

The Markstein length $\mathcal{L}_C$ appearing in the system 3 will be determined when justified to quantify the dependency of the burning velocity to the mean curvature $\mathcal{C} = \pm 1/R_V$.

4 Laminar flame results

Flame fronts of quasi-laminar spherical flames may be visualized on the first and fourth line of Fig. 1. Note that only the dry hydrogen flame become wrinkled. The expanding hydrogen flame looks like a 'soccer-ball' flame. Cells naturally emerge at large radii in expanding flames [23], nevertheless cellular disturbances are known to appear earlier in

[1] the open-source software 'paraview' (see http://paraview.org/) is used to analyse multi-bloc data.

the flame propagation process with negative Lewis numbers [24]. Similar instabilities were observed in the implosion case.

The time-evolution of the volume of fresh and burnt gases are respectively plotted for laminar implosions and explosions on Fig. 2. The flame area is not plotted since it follows the same trend. One can notice that internal volumes evolve faster at dry conditions

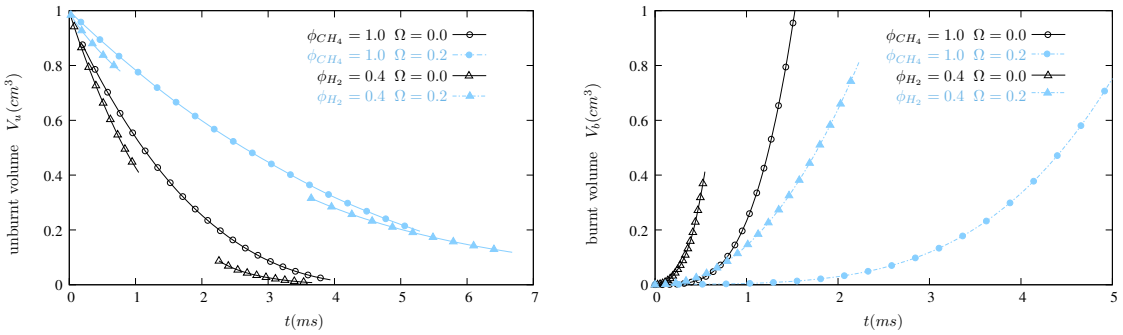

2a 2b

Figure 2. Time evolution of the internal volume delimited by the flame front for imploding (left) and expanding (right) laminar flames. This volume corresponds to fresh gases in implosions and to burnt gases in explosions.

since steam decreases the flame speed. They also increase faster in explosions that they decrease in implosions for a same mixture. This is due to the thermal expansion of fresh gases through the flame ($\rho_b dV_b = \rho_u dV_u \Rightarrow dV_b = T_b/T_u \cdot dV_u$). If fresh gases seem to be consumed at a similar speed whatever the fuel (methane or hydrogen) in implosions, burnt gases increase much faster with hydrogen in expanding flames (compare Fig. 2a to 2b). For further observations, the mean flame speed and consumption speed are plotted against the flame radius in the figure 3. The mean consumption speed is also plotted against the mean curvature and flame stretch.

As deduced from the previous curves, the figure 3a evidences that the flame moves much faster in expanding flames. It also shows a different behavior of flame expansion for the two fuels. Hydrogen expanding flames reach highest propagating speeds at smaller radii and slow down at larger radii. On the opposite, methane expanding flames accelerate as it is observed experimentally and numerically for propane flames [6, 9]. This behavior is observed both at dry and wet conditions. In imploding flames, methane imploding flames also seem to accelerate at smaller radii even if computations were not carried out till the end for cpu cost reasons. Note that Baillot *et* al. [10] observed experimentally such an acceleration (see red crosses in Fig. 3a). Quasi-spherical pockets of fresh gas were wrested into the burnt zone from a Bunsen burner operated in a pulsated mode. On the opposite, hydrogen imploding flames slow down as it was the case for expanding flames. The difference of behavior in hydrogen flames is attributed to the negative Lewis number of this fuel. This means that the mass diffusivity of hydrogen is higher than thermal diffusivity. Hydrogen may therefore diffuse in burnt gases to react with remaining oxygen and change the flame speed. Consumption speeds are significantly higher with H_2 than CH_4 in expansions (Fig. 3b). This explains why hydrogen expanding flames propagate faster than methane flames even if the thermal expansion is higher for methane flames.

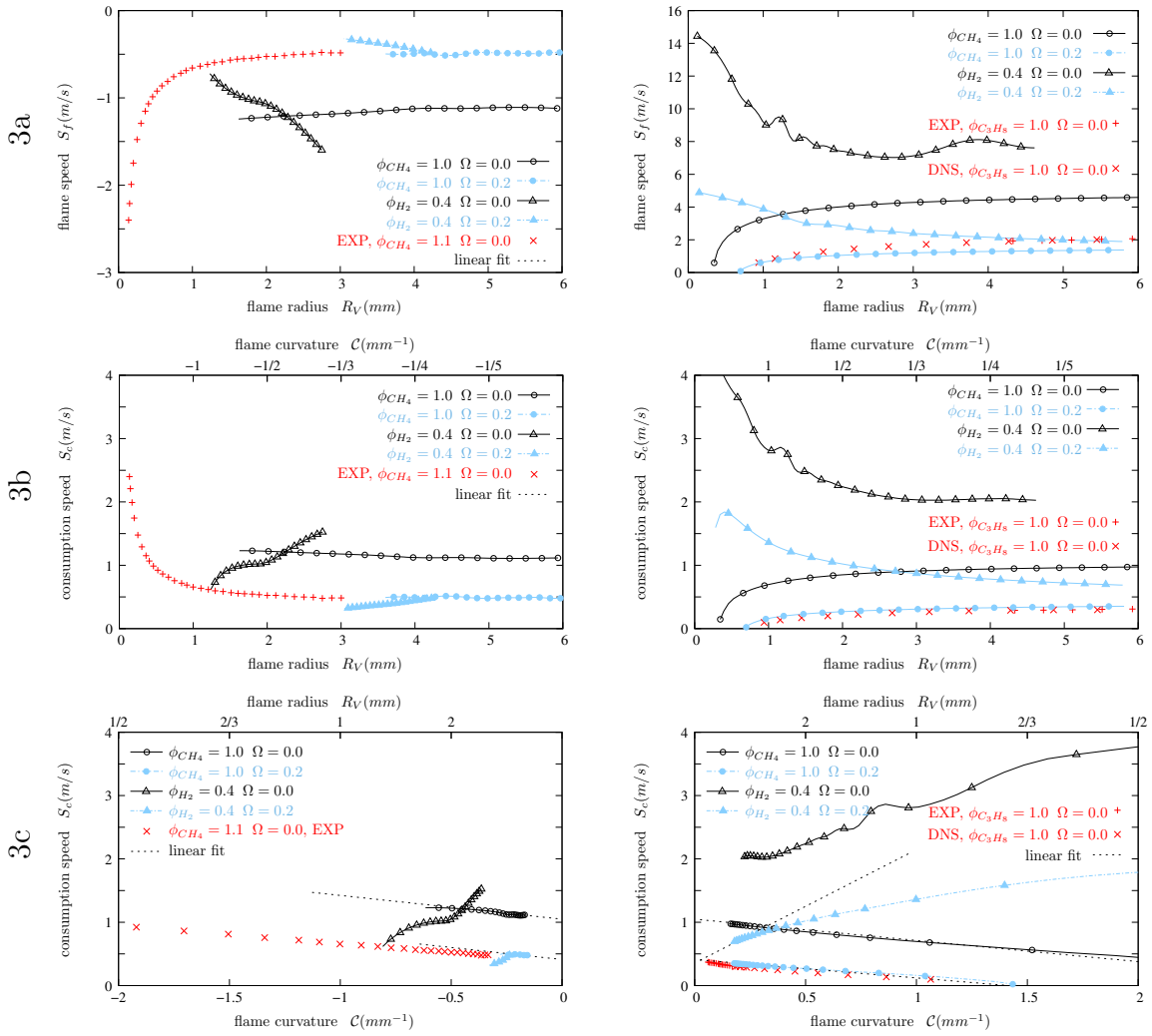

Figure 3. Representation of the mean flame speed and consumption speed along the mean flame radius or curvature for the different laminar imploding (left) and expanding (right) flames. Evolution from right to left in implosions and left to right in expansions.

In Fig. 3c, the linear link between consumption speeds and curvatures appears clearly, in particular for methane and propane fuels. Values of Markstein lengths defined by equations 3a and 3b are computed for all mixtures ($\mathcal{L}_{CH_4}^{\Omega=0} = 0.32mm$, $\mathcal{L}_{CH_4}^{\Omega=0.2} = 0.71mm$, $\mathcal{L}_{H_2}^{\Omega=0} = -1.2mm$, $\mathcal{L}_{H_2}^{\Omega=0.2} = -2.36mm$). The computed Markstein lengths of the dry methane cases are in good agreement with typical values obtained in [10, 6] with relative similar mixtures. Steam dilution increases Markstein lengths, which means that wet flames are more sensitive to curvature effects. This remark also holds on for negative Lewis numbers, even if curvature effects are inverted for negative and unity or positive Lewis numbers. With positive curvatures, consumption velocity then increases faster at wet conditions with unity or positive Lewis numbers of fuels like methane; on the opposite, it decreases faster in presence of steam with hydrogen.

5 Turbulent flame results

The effect of turbulence is directly visible on the flame fronts presented on the 2^{nd}, 3^{rd}, 5^{th} and last line of Fig. 1. Turbulence tends to wrinkle irregularly the flame front in all cases. Hydrogen dry flames seem once again significantly more wrinkled than other cases with smaller cell sizes, even if the integral length scale is the same for all simulations ($L_t = 3mm$). Steam seems to considerably decrease the flame wrinkles for a constant ratio between the initial rms velocity fluctuation and the flame speed. The same methodology as before is applied to investigate in more details the effect of turbulence on the propagation of these different flames. The time-evolution of the internal volumes of fresh or burnt gases is represented in Fig. 4a. The wrinkle ratio, defined as the ratio between the radii based on the flame area and the internal volume, is also plotted in Fig. 4b. The curves corresponding to laminar cases figure on the plots as dashed lines for comparisons with turbulent cases.

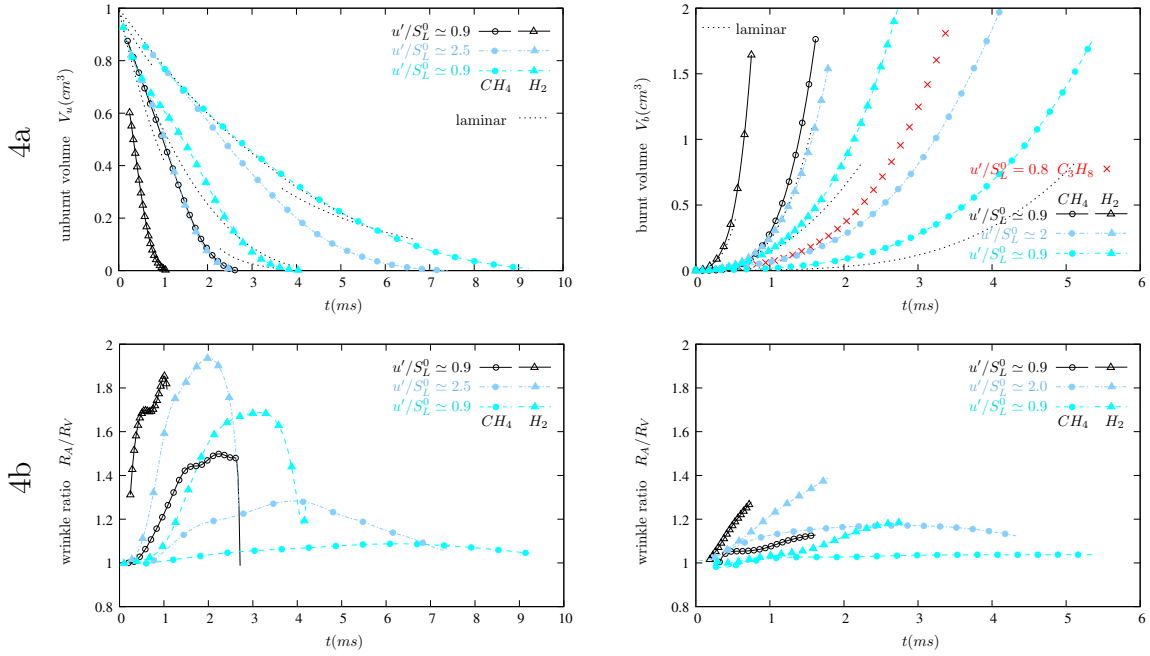

Figure 4. Time evolution of the internal volume and wrinkling ratio for the different imploding (left) and expanding (right) turbulent flames.

In most of cases, turbulence makes the internal volumes to evolve faster, except for the wet methane implosion case with the lowest turbulence intensity where no special difference is observed, compared to the laminar evolution. The acceleration of this evolution is particularly visible for hydrogen flames. The wrinkle ratio allows to quantify how much flames are wrinkled by comparing the growth of flame surface to its enclosed volume. In imploding flames, this wrinkling ratio is initially equal to one (perfect sphere) and increases before coming back to unity when the ultimate unburnt pocket disappears. In expanding flames, it increases till the end of simulations. It is apparent on Fig. 4b that flames are significantly more wrinkled in implosions than in expansions. For a nearly constant rms velocity fluctuation, flames present similar wrinkle ratio (compare dry cases with $u'/S_L^0 \simeq 0.9$ to wet cases with $u'/S_L^0 \simeq 2$), except maybe for the methane imploding

flame case. With a constant ratio u'/S_L^0, flames are significantly less wrinkled at high steam dilution.

The mean flame speed and consumption speed are once again plotted for these turbulent simulations in Fig. 5. The top right graph show that turbulent flames propagate

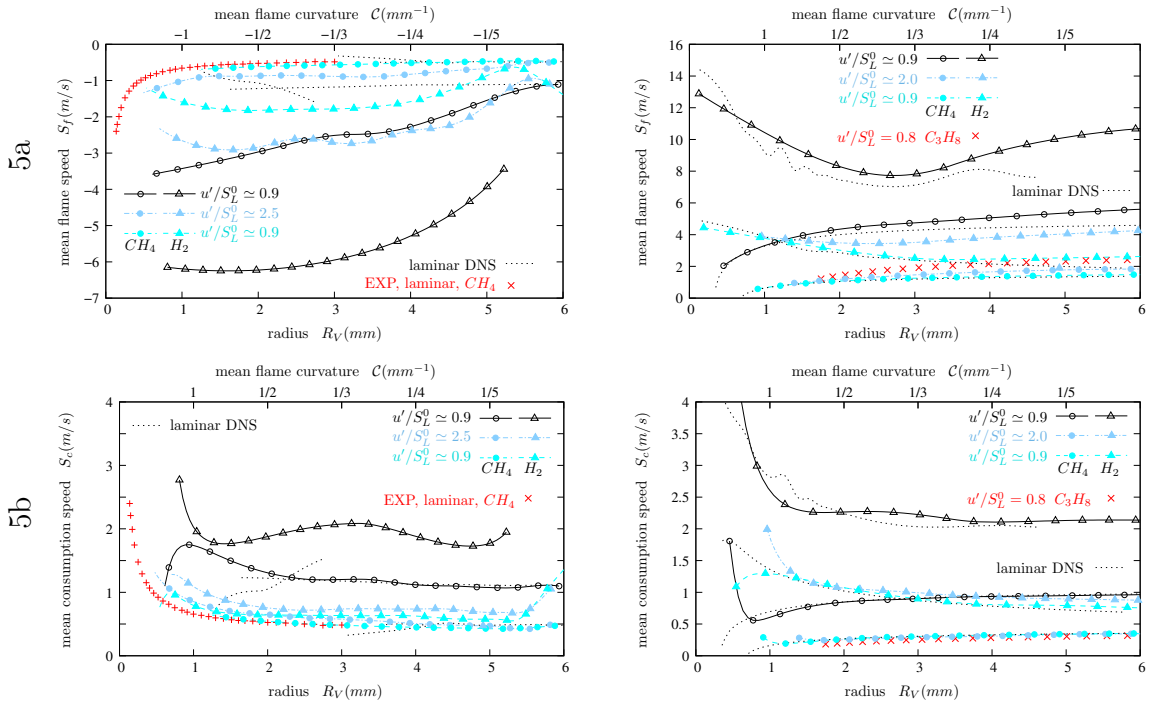

Figure 5. Representation of the mean flame speed and consumption speed along the mean flame radius, curvature or flame stretch for the different turbulent imploding (left) and expanding (right) flames. Evolution from right to left in implosions and left to right in expansions.

slightly faster than laminar flames at a given radius even if the consumption speed are quite identical for laminar and turbulent cases as indicated on the figure below (5b). In comparison, turbulent imploding flames are much faster than laminar ones for a same mixture. This is due to the fact that imploding flames are more wrinkled than expanding flames for a same initial turbulence. Indeed, equation 2 show that the flame speed is increased by the square of the wrinkling ratio that is larger for implosions. It is believed that the turbulence wrinkles less the expanding flame because the thermal expansion of gases pushes the fresh gases located near but outside the flame front. The flame acts as a piston that stretches the flow and decrease turbulent structures faster than in a free decaying isotropic turbulence. In the case of imploding flames, turbulent structures stay located inside the flame front and are then decaying freely ($u'(t) = u'_{ignition} \cdot \exp(-t/\tau)$ with $\tau \simeq 4ms$). For a same cpu-cost (see table 2), imploding flames allow to reach higher turbulent flame speed and larger wrinkle ratio than expanding flames.

If consumption speeds are not changed between turbulent and laminar implosions with methane fuel, an important increase of the burning velocity is noticeable with hydrogen fuel on the left graph of Fig. 5b. We believe that this sudden observed increase of the

burning velocity with turbulence is due the thermodiffusive instability. In flames with such a negative Lewis number, the thermodiffusive instability makes fuel to diffuse through the reactive interface. Much less hydrogen was observed in the cusps between flame cells. The reaction rate is highly decreased till extinction in these zones. This means that consumption speed considerably varies along the flame front and may explain that the averaged consumption speed on the flame front is not well defined for highly wrinkled flames with negative Lewis numbers. In the case of methane expanding flames, the reaction rate is relatively uniform along the flame front, which justifies that the mean consumption speed is a good estimation of the local consumption speed for methane flames.

6 Concluding remarks, future work

DNS of expanding and imploding flames were solved for stoichiometric methane-air and lean hydrogen-air mixtures at dry conditions or diluted with 20% of steam. Flames were ignited both in inert and turbulent flows. Main observations are summarized here below:

- Burning velocity and flame speeds depend significantly on the curvature of both laminar and turbulent flames, specially near smallest radii. The linear relation of Markstein was well verified and in good agreement with experimental results for unity or positive Lewis numbers.
- Flames in implosion were more wrinkled than expanding flames by turbulent structures, which makes imploding flames more suited to numerically reach higher wrinkle ratio in propagating flames.
- The thermodiffusive instability played a fundamental role in the propagation of hydrogen flames. Self wrinkling of the laminar flames appeared early only for the dry hydrogen flames, as observed experimentally. This instability increased considerably consumption and turbulent flame speeds of both wet and dry hydrogen flames compared to laminar propagations.
- Steam was found to thicken Markstein's length, which suggests that burning velocity of wet flames are more sensitive to curvature effects than dry flames. Steam nevertheless delayed the appearance of cellular disturbances due to the thermodiffusive instability, at least in laminar cases.
- For a constant turbulent intensity, wet flames were not significantly more wrinkled than dry flames even if steam brings the combustion closer to the regime of distributed reaction zones by thickening the flame. For a constant u'/S_L^0 ratio, steam significantly reduced flame wrinkles.
- The global analysis based on the observation of the total flame area and internal volume seemed to describe conveniently and satisfactorily the combustion except for highly wrinkled flames with negative Lewis numbers. A local analysis would help to quantify the accuracy of this global methodology. Analyses of the turbulent flow field would also help to better understand why explosions feel less the turbulence than implosions.

Acknowledgement

This work was granted access to the HPC resources of the RZG of the Max Planck Society made available within the Distributed European Computing Initiative by the PRACE-2IP, receiving funding from the European Community's Seventh Framework Programme

(FP7/2007-2013) under grant agreement n RI-283493. The research leading to these results has received funding from the European Research Council under the ERC grant agreement n ° 247322, GREENEST.

References

[1] S. Göke, K. Göckeler, O. Krüger, C. Paschereit, Computational and experimental study of premixed combustion at ultra wet conditions, ASME Turbo Expo 2010, ASME Paper 2010-GT-23417.

[2] M. Jonsson, J. Yan, Humidified gas turbines–a review of proposed and implemented cycles, Energy 30 (7) (2005) 1013–1078.

[3] S. Göke, C. Paschereit, Influence of steam dilution on NOx formation in premixed natural gas and hydrogen flames, 50$^{\text{th}}$ AIAA Aerospace Science Meeting, AIAA-2012-1272.

[4] V. Babkin, A. V'yun, Effect of water vapor on the normal burning velocity of a methane-air mixture at high pressures, Combustion, Explosion, and Shock Waves 7 (3) (1971) 339–341.

[5] E. Albin, H. Nawroth, S. Göke, Y. D'Angelo, C. Paschereit, Experimental investigation of burning velocities of ultra-wet methane–air–steam mixtures, Fuel Processing Technology 107 (2012) 27–35.

[6] B. Lecordier, Etude de l'interaction de la propagation d'une flamme prémélangée avec le champ aérodynamique, par association de la tomographie laser et de la vélocimétrie par images de particules, Ph.D. thesis (1997).

[7] E. Varea, V. Modica, A. Vandel, B. Renou, Measurement of laminar burning velocity and Markstein length relative to fresh gases using a new postprocessing procedure: Application to laminar spherical flames for methane, ethanol and isooctane/air mixtures, Combustion and Flame 159 (2) (2011) 577–590.

[8] J. Van Oijen, G. Groot, R. Bastiaans, L. de Goey, A flamelet analysis of the burning velocity of premixed turbulent expanding flames, Proceedings of the Combustion Institute 30 (1) (2005) 657–664.

[9] E. Albin, Y. DAngelo, Assessment of the Evolution Equation Modelling approach for three-dimensional expanding wrinkled premixed flames, Combustion and Flame 159 (5) (2012) 1932–1948.

[10] F. Baillot, D. Durox, D. Demare, Experiments on imploding spherical flames: effects of curvature, Proceedings of the Combustion Institute 29 (2) (2002) 1453–1460.

[11] D. Bradley, P. Gaskell, X. Gu, Burning velocities, markstein lengths, and flame quenching for spherical methane-air flames: a computational study, Combustion and Flame 104 (1) (1996) 176–198.

[12] G. R. A. Groot, Modelling of propagating spherical and cylindrical premixed flames, Ph.D. thesis (2003).

[13] M. Haq, C. Sheppard, R. Woolley, D. Greenhalgh, R. Lockett, Wrinkling and curvature of laminar and turbulent premixed flames, Combustion and flame 131 (1) (2002) 1–15.

[14] E. Albin, Y. DAngelo, Effects of Navier-Stokes characteristic outflow boundary conditions: modeling for transverse flows., Proceedings of ECM 2011, Cardiff.

[15] E. Albin, Y. D'Angelo, L. Vervisch, Using staggered grids with characteristic boundary conditions when solving compressible reactive navier–stokes equations, International Journal for Numerical Methods in Fluids 68 (5) (2011) 546–563.

[16] C. S. Yoo, H. G. Im, Characteristic boundary conditions for simulations of compressible reacting flows with multi-dimensional, viscous and reaction effects, Combustion Theory and Modelling 11 (2) (2007) 259–286.

[17] E. Albin, Y. DAngelo, L. Vervisch, Flow streamline based navier–stokes characteristic boundary conditions: Modeling for transverse and corner outflows, Computers & Fluids 51 (1) (2011) 115–126.

[18] S. Göke, M. Füri, G. Bourque, B. Bobusch, K. Göckeler, O. Krüger, S. Schimek, S. Terhaar, C. O. Paschereit, Influence of steam dilution on the combustion of natural gas and hydrogen in premixed and rich-quench-lean combustors, Fuel Processing Technology 107 (2012) 14–22.

[19] N. Babkovskaia, N. Haugen, A. Brandenburg, A high-order public domain code for direct numerical simulations of turbulent combustion, Journal of computational physics 230 (1) (2011) 1–12.

[20] M. D. Smooke, Reduced kinetic mechanisms and asymptotic approximations for methane-air flames: a topical volume, in: Reduced Kinetic Mechanisms and Asymptotic Approximations for Methane-Air Flames, Vol. 384, 1991.

[21] G. Smith, D. Golden, M. Frenklach, N. Moriarty, B. Eiteneer, M. Goldenberg, C. Bowman, R. Hanson, S. Song, W. Gardiner, V. Lissianski, Z. Qin, GRI-Mech 3.0, http://www.me.berkeley.edu/gri_mech/ (2000).

[22] M. Matalon, On flame stretch, Combustion Science and Technology 31 (3-4) (1983) 169–181.

[23] Y. D'angelo, G. Joulin, G. Boury, On model evolution equations for the whole surface of three-dimensional expanding wrinkled premixed flames, Combustion Theory and Modelling 4 (3) (2000) 317–338.

[24] K. Aung, M. Hassan, G. Faeth, Flame stretch interactions of laminar premixed hydrogen/air flames at normal temperature and pressure, Combustion and Flame 109 (1-2) (1997) 1–24.